Structural Engineering and Mechanics, Vol. 6, No. 6 (1998) 613-632
DOI: http://dx.doi.org/10.12989/sem.1998.6.6.613

Dynamic characteristics and response analysis of accelerating underwater structures

Zhengxing Liu†

Department of Engineering Mechanics, Shanghai Jiao Tong University, Shanghai 200030, China

F.W. Williams‡ and A.K. Jemah‡†

Division of Structural Engineering, Cardiff School of Engineering
Cardiff University, Cardiff, CF2 3TB, U.K.

Abstract. A coupling system for a structure accelerating through a fluid is considered which is composed of the structure and the fluid in a finite surrounding volume. Based on the variational principle, the finite element equations of hydrodynamic pressure and structural elastic vibration are deduced. A numerical method is given for the dynamic character and response of the structure which takes the coupled fluid into account. The effect of axial inertial forces on the dynamic character and response of rapidly accelerating structures is also considered.

Key words: structure/fluid interaction; dynamic response; added mass.

1. Introduction

In the early 19th Century, study of the rocking vibration of ships brought about the rapid development of the theory of fluid-solid coupling. Haskind (1946a, 1946b) was the first to establish a linear fluid dynamic theory. His contribution was to resolve the velocity potential of disturbance in the flow field into diffractive velocity potential and radiative velocity potential within the scope of linearity. This became a classical method for dealing with fluid-solid coupling.

Ursell (1949) used a multiple expansion method to investigate the boundary value problem of the velocity potential to obtain the force exerted by a fluid on a harmonically vibrating cylinder. The above methods form the foundation for the theory of fluid-solid coupling for ships, but are limited to phenomenal or qualitative analysis. It was not until the early 1950's, that substantial progress was achieved in analysing the interaction between ship and fluids, by using a slicing method.

Korvin-Kroukovsky and Jacobs (1957) used the concept of slender bodies in aerodynamics to propose an ordinary slicing method. A series of improvements followed, such as the reasonable slicing method of Ogilvie and Tuck (1969), and the method of Salvesen, *et al.*

† Visiting Professor in the Division of Structural Engineering of Cardiff University
‡ Professor
‡† Lecturer

(1970). These slicing methods are based on the assumption that the structure is slender. They give satisfactory results for a large range of velocities of conventional ships (Blok and Beukelman 1984), but are not accurate enough for high speed underwater vehicles. To account for the effect of velocity and for the fact that the structure is actually three dimensional, a unified slender-body theory was developed (Ursell 1962, Newman 1964) and was then steadily improved (Newman 1978a, 1978b, Mays 1978, Newman and Sclavounos 1980, Sclavounos 1981, 1984, 1985).

Despite successful applications of the slicing methods and of the unified slender-body theory, three-dimensional effects have attracted more and more attention due to the emergence of new ship structures and higher speeds. The investigation of such effects was successful for fixed offshore structures (Faltinsen and Michelsen 1974, Chang and Pien 1976, Korsmeyer *et al.* 1988 and Kagemoto and Yue 1993). Work has also been reported for ships travelling at conventional speeds (Chang 1977, Inglis and Price 1982 and Guevel and Bougis 1982). The results obtained were closer to experimental measurements than were those obtained by the slicing method, but were limited to the computation of three-dimensional flow fields, with no allowance for coupling with the elastic response of the structure.

Hydroelasticity is an important field for research on fluid-solid coupling, in which great progress was achieved in the 1970's (Bishop *et al.* 1973, Bishop and Price 1974 and Betts *et al.* 1977). These authors presented a two-dimensional linear beam slicing theory, in which the structure was modelled by a linear elastic Euler or Timoshenko beam and the flow field was approximated as being two-dimensional (Bishop and Price 1979). Two-dimensional hydroelasticity theory was also widely used in the 1980's (Bishop *et al.* 1984 and Clark 1986).

Since the late 1980's, much research has been carried out using three-dimensional hydroelasticity, including theory (Wu 1984) and applications (Lundgren *et al.* 1988 and Ertekin *et al.* 1993). However, there is still a lack of reported research on fluid-solid coupling for accelerating underwater structures. This paper addresses this shortcoming as follows.

An elastic structure accelerating through a fluid medium vibrates when it is subjected to hydrodynamic load. Its vibration induces additional hydrodynamic load through its interface with the fluid. This process leads to coupled fluid-structure response. The effect of axial forces on the dynamic characteristics and response are optionally considered. It is difficult to analyse such problems precisely, because so many complex factors are involved (Lamb 1920). Therefore, this paper uses fluid mechanics, elastic mechanics and the variational principle to derive engineering analysis methods.

2. Hydrodynamic pressure

The distribution of hydrodynamic pressure of an accelerating underwater structure is very complex and the additional hydrodynamic pressure induced by structural vibrations is very small compared to the total hydrodynamic pressure. Therefore, only incompressible fluid and small amplitude vibrations are considered. Hence the hydrodynamic fluid pressure P satisfies the equations

$$\text{In } V: \qquad \frac{\partial^2 P}{\partial X^2} + \frac{\partial^2 P}{\partial Y^2} + \frac{\partial^2 P}{\partial Z^2} = 0$$

$$\text{On } S_p: \qquad P = \overline{P}$$

$$\text{On } S_n: \quad \frac{\partial P}{\partial n} = -\rho \frac{\partial^2 u_n}{\partial t^2} \tag{1}$$

where: V is the volume of surrounding fluid taken into account, see Fig. 1, which will be looked at in more detail later and which shows a typical underwater plane beam and its finite element mesh, for which $V = 2l \times l \times 0.1l$; S_n is the fluid-structure interface; $S_p \cup S_n$ is the boundary of the fluid; $\bar{P}$ is a given hydrodynamic pressure; n is a normal to the fluid interface acting from the fluid to the structure; u_n is the (normal) displacement along n and; ρ is the density of the fluid.

The functional that corresponds to Eq. (1) is (Zienkiewicz 1977)

$$\Pi = \int_V \frac{1}{2}\left[\left(\frac{\partial P}{\partial X}\right)^2 + \left(\frac{\partial P}{\partial Y}\right)^2 + \left(\frac{\partial P}{\partial Z}\right)^2\right] dV + \int_{S_n} \left(\rho \frac{\partial^2 u_n}{\partial t^2}\right) P dS \tag{2}$$

If the fluid region is represented by N_E accelerating elements, which are assembled such that the usual equilibrium and compatibility conditions of the finite element method are satisfied at the nodes, then Eq. (2) may be written as

$$\Pi = \sum_{e=1}^{N_E} \Pi_e$$

where

$$\Pi_e = \int_{V_e} \frac{1}{2}\left[\left(\frac{\partial P}{\partial X}\right)^2 + \left(\frac{\partial P}{\partial Y}\right)^2 + \left(\frac{\partial P}{\partial Z}\right)^2\right] dV + \int_{S_{ne}} \rho \frac{\partial^2 u_n}{\partial t^2} P dS \tag{3}$$

and subscript e represents a typical element of the fluid, e.g., see Fig. 2, which will be looked at in more detail later and which shows a typical triangular element, taken in this case from Fig. 1.

The hydrodynamic pressure in the fluid element may be represented as

$$P = \underset{\sim}{N}\underset{\sim}{q}_e \tag{4}$$

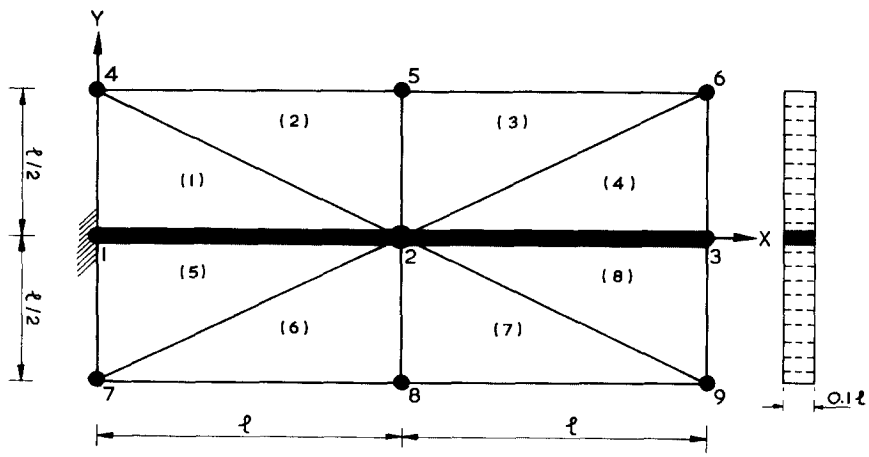

Fig. 1 An underwater plane beam and its finite element mesh

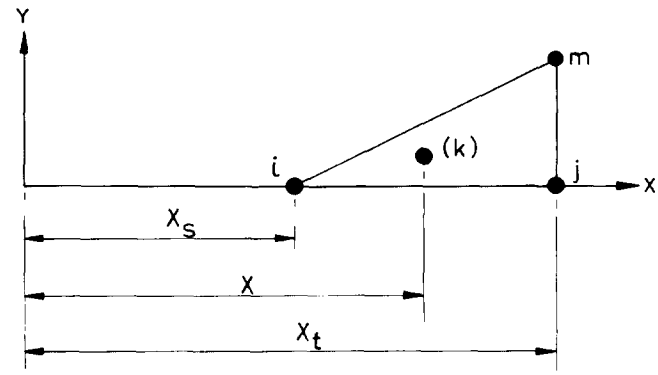

Fig. 2 A typical fluid element

and the normal displacement at the element interface may be expressed as

$$u_n = \underset{\sim}{N}_S \, \underset{\sim}{d}_{ne} \tag{5}$$

where $\underset{\sim}{N}$ and $\underset{\sim}{N}_S$ are interpolation functions defined in V_e and on S_{ne} and $\underset{\sim}{q}_e$ ***and*** $\underset{\sim}{d}_{ne}$ are respectively the hydrodynamic pressure and normal displacement vectors at the nodes of the element. After substituting Eqs. (4) and (5) into Eq. (3) and taking its stationary value, the fundamental equation of a fluid element becomes

$$\underset{\sim}{H}_e \underset{\sim}{q}_e = \underset{\sim}{F}_e = -\underset{\sim}{B}_{Se} \ddot{\underset{\sim}{d}}_{ne} \tag{6}$$

where $\ddot{\underset{\sim}{d}}_{ne}$ is the normal displacement acceleration of the node on the interface and

$$\underset{\sim}{H}_e = \int_{V_e} \left(\frac{\partial}{\partial X} \underset{\sim}{N}^T \frac{\partial}{\partial X} \underset{\sim}{N} + \frac{\partial}{\partial Y} \underset{\sim}{N}^T \frac{\partial}{\partial Y} \underset{\sim}{N} + \frac{\partial}{\partial Z} \underset{\sim}{N}^T \frac{\partial}{\partial Z} \underset{\sim}{N} \right) dV$$

$$\underset{\sim}{B}_{Se} = \int_{S_{ne}} \underset{\sim}{N}^T \rho \underset{\sim}{N}_S \, dS \tag{7}$$

By using the equilibrium requirement of hydrodynamic pressure and compatibility for an accelerating structure, the fundamental equation for the whole fluid region may be assembled as

$$\underset{\sim}{H} \underset{\sim}{Q} = \underset{\sim}{F} = -\underset{\sim}{B} \ddot{\underset{\sim}{D}}_S \tag{8}$$

where $\underset{\sim}{Q}$, $\underset{\sim}{F}$ and $\ddot{\underset{\sim}{D}}_S$ are vectors of, respectively, the hydrodynamic pressure of the nodes, the equivalent node loads and the normal acceleration of the nodes.

3. The hydrodynamic pressure on the contact interface

Partitioning the hydrodynamic pressure of the nodes into three parts gives

$$\underset{\sim}{Q} = \begin{bmatrix} \underset{\sim}{Q}_p \\ \underset{\sim}{Q}_n \\ \underset{\sim}{Q}_v \end{bmatrix} \tag{9}$$

where $\underset{\sim}{Q}_p$, $\underset{\sim}{Q}_n$ and $\underset{\sim}{Q}_v$ are the hydrodynamic pressures of nodes, respectively, on the

boundaries S_p and S_n and elsewhere in the fluid. Partitioning Eq. (8) accordingly gives

$$\begin{bmatrix} \underset{\sim}{H}_{pp} & \underset{\sim}{H}_{pn} & \underset{\sim}{H}_{pv} \\ \underset{\sim}{H}_{np} & \underset{\sim}{H}_{nn} & \underset{\sim}{H}_{nv} \\ \underset{\sim}{H}_{vp} & \underset{\sim}{H}_{vn} & \underset{\sim}{H}_{vv} \end{bmatrix} \begin{bmatrix} \underset{\sim}{Q}_p \\ \underset{\sim}{Q}_n \\ \underset{\sim}{Q}_v \end{bmatrix} = \begin{bmatrix} \underset{\sim}{F}_p \\ \underset{\sim}{F}_n \\ \underset{\sim}{F}_v \end{bmatrix} = - \begin{bmatrix} \underset{\sim}{B}_p \\ \underset{\sim}{B}_n \\ \underset{\sim}{B}_v \end{bmatrix} \ddot{\underset{\sim}{D}}_S$$

The above equation can be solved when $\underset{\sim}{Q}_p$ is given on S_p. If S_p is placed sufficiently far from the structure, it can be assumed that the hydrodynamic pressure on S_p has no influence on the structure, i.e., $\underset{\sim}{Q}_p=\underset{\sim}{0}$. Therefore the above equation can be solved conveniently under this assumption. Hence the fundamental equation for $\underset{\sim}{Q}_n$ may be obtained as

$$\underset{\sim}{H}_N \underset{\sim}{Q}_n = \underset{\sim}{F}_N = - \underset{\sim}{B}_N \ddot{\underset{\sim}{D}}_S$$

i.e.,

$$\underset{\sim}{Q}_n = - \underset{\sim}{H}_N^{-1} \underset{\sim}{B}_N \ddot{\underset{\sim}{D}}_S \tag{10}$$

in which

$$\begin{aligned} \underset{\sim}{H}_N &= \underset{\sim}{H}_{nn} - \underset{\sim}{H}_{nv} \underset{\sim}{H}_{vv}^{-1} \underset{\sim}{H}_{vn} \\ \underset{\sim}{F}_N &= \underset{\sim}{F}_n - \underset{\sim}{H}_{nv} \underset{\sim}{H}_{vv}^{-1} \underset{\sim}{F}_v \\ \underset{\sim}{B}_N &= \underset{\sim}{B}_n - \underset{\sim}{H}_{nv} \underset{\sim}{H}_{vv}^{-1} \underset{\sim}{B}_v \end{aligned} \tag{11}$$

The $\underset{\sim}{Q}_v$, which is needed to analyse the fluid field, may also be obtained as

$$\underset{\sim}{Q}_v = \underset{\sim}{H}_{vv}^{-1} (\underset{\sim}{F}_v - \underset{\sim}{H}_{vn} \underset{\sim}{Q}_n) \tag{12}$$

4. Equivalent node load

Introducing a location matrix $\underset{\sim}{A}_k$, the hydrodynamic pressure of the nodes on the structure-fluid interface of the k-th element can be found from $\underset{\sim}{Q}_n$ as

$$\underset{\sim}{q}_k = \underset{\sim}{A}_k \underset{\sim}{Q}_n \qquad k = 1, 2, \cdots, S_E \tag{13}$$

where S_E is the number of structure elements in contact with the fluid. Then the hydrodynamic pressure on the contact interface may be represented by

$$P_k = \underset{\sim}{N}_{Sk} \underset{\sim}{q}_k = \underset{\sim}{N}_{Sk} \underset{\sim}{A}_k \underset{\sim}{Q}_n, \qquad k = 1, 2, \cdots, S_E \tag{14}$$

Applying a virtual displacement δu_n normal to the contact interface and using Eq. (5) gives the virtual work of P_k as

$$\delta W = \int_{S_{nk}} \delta u_u^T P_k \, dS = \delta \underset{\sim}{d}_{nk}^T \int_{S_{nk}} \underset{\sim}{N}_{Sk}^T P_k \, dS$$

Assuming that the ordering of the equivalent node load vector $\underset{\sim}{F}_{ek}$ is consistent with $\underset{\sim}{q}_k$ and that its directions are consistent with $\underset{\sim}{d}_{nk}$, gives

$$\delta W = \delta \underset{\sim}{d}_{nk}^T \underset{\sim}{F}_{ek}$$

Comparing the above two equations shows that the equivalent node loads may be obtained as

$$\underset{\sim}{F}_{ek} = \int_{S_{nk}} \underset{\sim}{N}_{Sk}^T P_k \, dS, \qquad k = 1, 2, \cdots, S_E \tag{15}$$

Similarly, assuming that the ordering of the equivalent node load vector $\underset{\sim}{F}_Q$ at all nodes on the contact interface is consistent with $\underset{\sim}{Q}_n$, the location of each element of $\underset{\sim}{F}_{ek}$ in the $\underset{\sim}{F}_Q$ may be written as

$$\underset{\sim}{F}_{Qk} = \underset{\sim}{A}_k^T \underset{\sim}{F}_{ek}, \qquad k = 1, 2, \cdots, S_E \tag{16}$$

After applying Eq. (16) to every element on the interface, the equivalent node load induced by additional hydrodynamic pressure may be calculated as

$$\underset{\sim}{F}_Q = \sum_{k=1}^{S_E} \underset{\sim}{F}_{Qk} = \sum_{k=1}^{S_E} \underset{\sim}{A}_k^T \underset{\sim}{F}_{ek} \tag{17}$$

Substituting Eqs. (15), (14) and (10) into Eq. (17) yields

$$\underset{\sim}{F}_Q = -\underset{\sim}{M}_P \ddot{\underset{\sim}{D}}_S \tag{18}$$

where $\underset{\sim}{M}_P$ is the *additional water mass matrix* given by

$$\underset{\sim}{M}_P = \left(\sum_{k=1}^{S_E} \underset{\sim}{A}_k^T \underset{\sim}{L}_k \underset{\sim}{A}_k \right) \underset{\sim}{H}_N^{-1} \underset{\sim}{B}_N \tag{19}$$

where

$$\underset{\sim}{L}_k = \int_{S_{nk}} \underset{\sim}{N}_{Sk}^T \underset{\sim}{N}_{Sk} \, dS$$

A co-ordinate transformation is necessary before using Eq. (18) in the analysis of the structure, as follows.

A common global structural co-ordinate system $(\bar{X}\bar{Y}\bar{Z})$ and positive normal n_A of a node A located on the interface of the structure and the fluid are given in Fig. 3. The normal displacement of node A may be written as

$$u_{n(A)} = [\cos(n_A \bar{X}) \quad \cos(n_A \bar{Y}) \quad \cos(n_A \bar{Z})] \begin{bmatrix} \bar{u}_A \\ \bar{v}_A \\ \bar{w}_A \end{bmatrix} = \underset{\sim}{T}_A \underset{\sim}{\bar{d}}_A$$

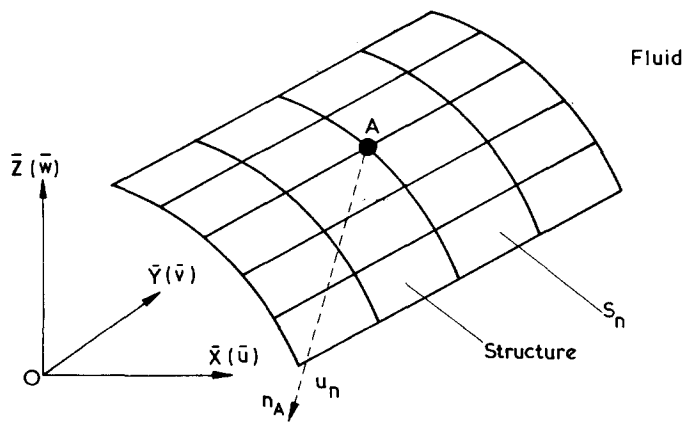

Fig. 3 Structure-fluid system

where $(n_A \bar{X})$ represents the angle between the normal n_A and the $\bar{X}$ axis, etc.

The ordering for all nodes located on the contact interface may be represented as

$$\begin{bmatrix} u_{n(1)} \\ u_{n(2)} \\ \cdot \\ \cdot \\ \cdot \\ u_{n(g)} \end{bmatrix} = \begin{bmatrix} \underset{\sim}{T}_1 & & & & \\ & \underset{\sim}{T}_2 & & & \\ & & \cdot & & \\ & & & \cdot & \\ & & & & \underset{\sim}{T}_g \end{bmatrix} \begin{bmatrix} \bar{\underset{\sim}{d}}_1 \\ \bar{\underset{\sim}{d}}_2 \\ \cdot \\ \cdot \\ \cdot \\ \bar{\underset{\sim}{d}}_g \end{bmatrix}$$

which may be written as

$$\underset{\sim}{D}_S = \underset{\sim}{\Lambda} \bar{\underset{\sim}{D}}_S \tag{20}$$

The node load and the normal acceleration of the node have the same transformation relationship i.e.,

$$\underset{\sim}{F}_Q = \underset{\sim}{\Lambda} \underset{\sim}{F}_Q, \qquad \ddot{\underset{\sim}{D}}_S = \underset{\sim}{\Lambda} \ddot{\bar{\underset{\sim}{D}}}_S \tag{21}$$

Substituting Eqs. (20) and (21) into Eq. (18) and introducing the well-known property of the transformation matrix $\underset{\sim}{\Lambda}$, i.e.

$$\underset{\sim}{\Lambda} \underset{\sim}{\Lambda}^T = \underset{\sim}{I}$$

where $\underset{\sim}{I}$ is a unit matrix, gives the equivalent node load vector in the global co-ordinate system as

$$\bar{\underset{\sim}{F}}_Q = -\bar{\underset{\sim}{M}}_P \ddot{\bar{\underset{\sim}{D}}}_S \tag{22}$$

where

$$\bar{\underset{\sim}{M}}_P = \underset{\sim}{\Lambda}^T \underset{\sim}{M}_P \underset{\sim}{\Lambda} \tag{23}$$

5. The dynamic equation of the structure

The discretized dynamic equations of the structure in the global co-ordinate system can be written as

$$\bar{\underset{\sim}{M}} \ddot{\bar{\underset{\sim}{D}}} + \bar{\underset{\sim}{C}} \dot{\bar{\underset{\sim}{D}}} + \bar{\underset{\sim}{K}} \bar{\underset{\sim}{D}} = \bar{\underset{\sim}{F}}_S + \bar{\underset{\sim}{F}}_G \tag{24}$$

where $\bar{\underset{\sim}{M}}$, $\bar{\underset{\sim}{C}}$ and $\bar{\underset{\sim}{K}}$ are, respectively, the mass matrix, damping matrix and stiffness matrix of the structure, while $\bar{\underset{\sim}{D}}$ is the degrees-of-freedom of the nodes of the assembled structure. $\bar{\underset{\sim}{F}}_S$ contains those parts of the node loads which are induced by additional hydrodynamic pressure while $\bar{\underset{\sim}{F}}_G$ contains the other node loads, which are applied directly to the structure.

$\bar{\underset{\sim}{D}}$ can be partitioned as

$$\bar{\underset{\sim}{D}} = \begin{bmatrix} \bar{\underset{\sim}{D}}_S \\ \bar{\underset{\sim}{D}}_t \end{bmatrix} \tag{25}$$

where the elements of $\overline{\underset{\sim}{D}}_S$ are called the *moisture degrees-of-freedom*, which are located on the structure/fluid interface and $\overline{\underset{\sim}{D}}_t$ contains the remaining *dry degrees-of-freedom*. Because the order of matrix $\overline{\underset{\sim}{F}}_S$ differs from that of $\overline{\underset{\sim}{F}}_Q$, it is necessary to introduce

$$\overline{\underset{\sim}{F}}_S = \begin{bmatrix} \overline{\underset{\sim}{F}}_Q \\ \underset{\sim}{0} \end{bmatrix} = - \begin{bmatrix} \overline{\underset{\sim}{M}}_P & \underset{\sim}{0} \\ \underset{\sim}{0} & \underset{\sim}{0} \end{bmatrix} \begin{bmatrix} \ddot{\overline{\underset{\sim}{D}}}_S \\ \ddot{\overline{\underset{\sim}{D}}}_t \end{bmatrix}$$

i.e.,

$$\overline{\underset{\sim}{F}}_S = - \overline{\underset{\sim}{M}}_G \ddot{\overline{\underset{\sim}{D}}} \tag{26}$$

Substituting Eq. (26) into Eq. (24) and rearranging gives

$$(\overline{\underset{\sim}{M}} + \overline{\underset{\sim}{M}}_G) \ddot{\overline{\underset{\sim}{D}}} + \overline{\underset{\sim}{C}} \dot{\overline{\underset{\sim}{D}}} + \overline{\underset{\sim}{K}} \overline{\underset{\sim}{D}} = \overline{\underset{\sim}{F}}_G \tag{27}$$

This is the fundamental dynamic equation for the structural analysis which includes the influence of the fluid. For natural vibrations, Eq. (27) becomes

$$(\overline{\underset{\sim}{M}} + \overline{\underset{\sim}{M}}_G) \ddot{\overline{\underset{\sim}{D}}} + \overline{\underset{\sim}{C}} \dot{\overline{\underset{\sim}{D}}} + \overline{\underset{\sim}{K}} \overline{\underset{\sim}{D}} = \underset{\sim}{0} \tag{28}$$

If damping is not considered, Eq. (28) simplifies to

$$(\overline{\underset{\sim}{M}} + \overline{\underset{\sim}{M}}_G) \ddot{\overline{\underset{\sim}{D}}} + \overline{\underset{\sim}{K}} \overline{\underset{\sim}{D}} = \underset{\sim}{0} \tag{29}$$

In this paper, the subspace iteration method is adopted to solve the natural vibration Eqs. (28) or (29) and the method of superposition of vibration modes is adopted to solve the dynamic response Eq. (27).

6. The effect of axial inertia forces

Consider an accelerating column of length l subjected to an axial force F at its end n, see Fig. 4. The acceleration of the column is

$$a = \frac{F}{M} \tag{30}$$

where M is the total mass of the column. If the column is divided into n elements and n+1 nodes, as shown in Fig. 4, then the axial inertia force on the i-th element may be

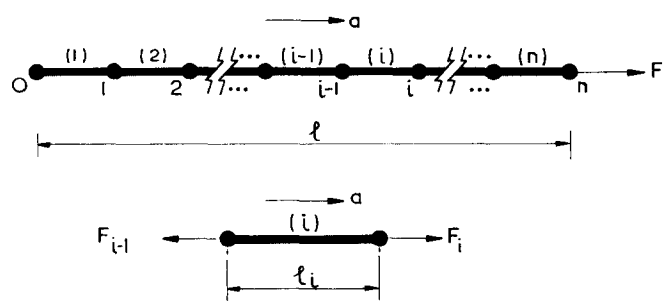

Fig. 4 Slender column in axial motion

approximately defined as

$$F_i = F_{i-1} + \frac{m_i}{M} F, \qquad i = 1, 2, \cdots, n. \tag{31}$$

where m_i is the mass of the i-th element and $F_0=0$, $F_n=F$ and $M=\Sigma m_i$.

The effect of the axial force F_i can be called the *geometric stiffness matrix* (Holand and Bell 1972, Kabaila 1970). For example, for a plane beam element it may be defined as

$$\underset{\sim}{\boldsymbol{k}}_G = \frac{F}{l} \begin{bmatrix} \frac{6}{5} & & \textit{symmetric} & \\ \frac{l}{10} & \frac{2l^2}{15} & & \\ \frac{-6}{5} & \frac{-l}{10} & \frac{6}{5} & \\ \frac{l}{10} & \frac{-l^2}{30} & \frac{-l}{10} & \frac{2l^2}{15} \end{bmatrix} \tag{32}$$

Thus, the stiffness matrix $\overline{\underset{\sim}{K}}$ in Eqs. (27), (28) and (29) is assembled by including all the element matrices i.e., $\overline{\underset{\sim}{K}}$ becomes $\overline{\underset{\sim}{K}}+\overline{\underset{\sim}{K}}_G$, where $\overline{\underset{\sim}{K}}_G$ is the result of assembling all of the $\underset{\sim}{\boldsymbol{k}}_G$.

7. Numerical examples

7.1. Example 1

Fig. 1 shows a plane cantilever beam of length $L=2l$ and width $0.1l$ immersed in water and with a global X-Y co-ordinate system. The water volume is taken as $2l \times l \times 0.1l$ with thickness $h=0.1l$. For the numerical calculations $l=0.1$m, the beam was divided into 2 plane beam elements and the water region was divided into 8 plane triangular elements, giving the 9 nodes shown for the coupled structure/water system of which the first three are located at the structure/water interface.

The cross-sectional area of the beam $\bar{A}=0.0002\text{m}^2$ and its second moment of area $J=\frac{2}{3}\times 10^{-8}\text{m}^4$. Young's modulus $E=200$ GN/m^2, density $\rho_b=10^4$ kg/m^3 and the water density $\rho=10^3$ kg/m^3. Note that the values chosen here are only approximately correct for real materials, having been rounded to convenient values to make the following calculations easy to follow. Similarly, although the beam depth of $0.2l$ (=0.02m) is quite large it has been treated as small by the water finite element mesh of Fig. 1.

The k-th fluid element is used to illustrate the application of the method presented in this paper, as shown in Fig. 2 with $k=4$.

The interpolations $\underset{\sim}{N}$ and $\underset{\sim}{N}_S$ are taken, respectively, as (Przemieniecki 1968)

$$\underset{\sim}{\boldsymbol{N}} = [N_i \; N_j \; N_m]$$

$$N_i = (a_i + b_i X + c_i Y)/2A$$

$$a_i = X_j Y_m - Y_j X_m, \quad b_i = Y_j - Y_m, \quad C_i = X_m - X_j \quad (i.j.m)$$

$$\underset{\sim}{N}_S = [X_t - X \quad X - X_s]/(X_t - X_s)$$

where A is the plane area of the triangular element. Eq. (7) gives $\underset{\sim}{H}_k$ and $\underset{\sim}{B}_{Sk}$ as

$$\underset{\sim}{H}_k = h\int_{S_k}\left(\frac{\partial}{\partial X}\underset{\sim}{N}^T\frac{\partial}{\partial X}\underset{\sim}{N}+\frac{\partial}{\partial Y}\underset{\sim}{N}^T\frac{\partial}{\partial Y}\underset{\sim}{N}\right)dxdy$$

$$= \frac{h}{4A}\left(\begin{bmatrix} b_i^2 & b_ib_j & b_ib_m \\ b_jb_i & b_j^2 & b_jb_m \\ b_mb_i & b_mb_j & b_m^2 \end{bmatrix} + \begin{bmatrix} C_i^2 & C_iC_j & C_iC_m \\ C_jC_i & C_j^2 & C_jC_m \\ C_mC_i & C_mC_j & C_m^2 \end{bmatrix}\right)$$

$$\underset{\sim}{B}_{Sk} = \int_{S_{nk}}\underset{\sim}{N}^T\rho\underset{\sim}{N}_S\,dS = \frac{\rho h}{X_t - X_s}\int\underset{\sim}{N}^T[X_t - X \quad X - X_s]\,dX$$

$$= \frac{\rho h}{2Al}\left(\begin{bmatrix} a_iX_t^2+\frac{1}{2}(b_iX_t-a_i)X_t^2-\frac{1}{3}b_iX_t^3 & -a_iX_sX_t+\frac{1}{2}(a_i-X_sb_i)X_t^2+\frac{1}{3}b_iX_t^3 \\ a_jX_t^2+\frac{1}{2}(b_jX_t-a_j)X_t^2-\frac{1}{3}b_jX_t^3 & -a_jX_sX_t+\frac{1}{2}(a_j-X_sb_j)X_t^2+\frac{1}{3}b_jX_t^3 \\ a_mX_t^2+\frac{1}{2}(b_mX_t-a_m)X_t^2-\frac{1}{3}b_mX_t^3 & -a_mX_sX_t+\frac{1}{2}(a_m-X_sb_m)X_t^2+\frac{1}{3}b_mX_t^3 \end{bmatrix}\right.$$

$$\left. - \begin{bmatrix} a_iX_tX_s+\frac{1}{2}(b_iX_t-a_i)X_s^2-\frac{1}{3}b_iX_s^3 & -a_iX_s^2+\frac{1}{2}(a_i-X_sb_i)X_s^2+\frac{1}{3}b_iX_s^3 \\ a_jX_tX_s+\frac{1}{2}(b_jX_t-a_j)X_s^2-\frac{1}{3}b_jX_s^3 & -a_jX_s^2+\frac{1}{2}(a_j-X_sb_j)X_s^2+\frac{1}{3}b_jX_s^3 \\ a_mX_tX_s+\frac{1}{2}(b_mX_t-a_m)X_s^2-\frac{1}{3}b_mX_s^3 & -a_mX_s^2+\frac{1}{2}(a_m-X_sb_m)X_s^2+\frac{1}{3}b_mX_s^3 \end{bmatrix}\right)$$

Inserting numerical values into the above and treating the triangular elements in the order k= 1, 2, ···, 8 enables Eq. (8) to be written (using the order $\underset{\sim}{Q}_n$, $\underset{\sim}{Q}_p$ instead of $\underset{\sim}{Q}_p$, $\underset{\sim}{Q}_n$ for

$$\begin{bmatrix} 250 & -50 & 0 & -100 & 0 & 0 & -100 & 0 & 0 \\ -50 & 500 & -50 & 0 & -200 & 0 & 0 & -200 & 0 \\ 0 & -50 & 250 & 0 & 0 & -100 & 0 & 0 & -100 \\ -100 & 0 & 0 & 125 & -25 & 0 & 0 & 0 & 0 \\ 0 & -200 & 0 & -25 & 250 & -25 & 0 & 0 & 0 \\ 0 & 0 & -100 & 0 & -25 & 125 & 0 & 0 & 0 \\ -100 & 0 & 0 & 0 & 0 & 0 & 125 & -25 & 0 \\ 0 & -200 & 0 & 0 & 0 & 0 & -25 & 250 & -25 \\ 0 & 0 & -100 & 0 & 0 & 0 & 0 & -25 & 125 \end{bmatrix} \begin{bmatrix} q_1 \\ q_2 \\ q_3 \\ q_4 \\ q_5 \\ q_6 \\ q_7 \\ q_8 \\ q_9 \end{bmatrix}$$

convenience) as

$$= \frac{-10^3 \rho}{3} \begin{bmatrix} 2 & 1 & 0 \\ 1 & 4 & 1 \\ 0 & 1 & 2 \\ 0 & 0 & 0 \\ 0 & 0 & 0 \\ 0 & 0 & 0 \\ 0 & 0 & 0 \\ 0 & 0 & 0 \\ 0 & 0 & 0 \end{bmatrix} \begin{bmatrix} \ddot{d}_{n1} \\ \ddot{d}_{n2} \\ \ddot{d}_{n3} \end{bmatrix}$$

Because $\underset{\sim}{Q}_v$ and $\underset{\sim}{Q}_p$ are neglected in this example, so that $\underset{\sim}{Q}_v = \underset{\sim}{Q}_p = \underset{\sim}{0}$, Eq. (10) becomes

$$\begin{bmatrix} 250 & -50 & 0 \\ -50 & 500 & -50 \\ 0 & -50 & 250 \end{bmatrix} \begin{bmatrix} q_1 \\ q_2 \\ q_3 \end{bmatrix} = \frac{-10^3 \rho}{3} \begin{bmatrix} 2 & 1 & 0 \\ 1 & 4 & 1 \\ 0 & 1 & 2 \end{bmatrix} \begin{bmatrix} \ddot{d}_{n1} \\ \ddot{d}_{n2} \\ \ddot{d}_{n3} \end{bmatrix}$$

which has the solution

$$\begin{bmatrix} q_1 \\ q_2 \\ q_3 \end{bmatrix} = -\frac{\rho}{36} \left(\begin{bmatrix} 103 & 70 & 7 \\ 35 & 110 & 35 \\ 7 & 70 & 103 \end{bmatrix} \right) \begin{bmatrix} \ddot{d}_{n1} \\ \ddot{d}_{n2} \\ \ddot{d}_{n3} \end{bmatrix}$$

which can be written as Eq. (10), i.e.,

$$\underset{\sim}{Q}_n = -\underset{\sim}{H}_N^{-1} \underset{\sim}{B}_N \ddot{\underset{\sim}{D}}_S$$

It is obvious that the location matrices in this example are

$$\underset{\sim}{A}_1 = \begin{bmatrix} 1 & 0 & 0 \\ 0 & 1 & 0 \end{bmatrix}, \quad \underset{\sim}{A}_2 = \begin{bmatrix} 0 & 1 & 0 \\ 0 & 0 & 1 \end{bmatrix}$$

By using Eq. (19), $\underset{\sim}{L}_1$, $\underset{\sim}{L}_2$ and $\underset{\sim}{M}_P$ are found to be

$$\underset{\sim}{L}_1 = \frac{lh}{6} \begin{bmatrix} 2 & 1 \\ 1 & 2 \end{bmatrix}, \quad \underset{\sim}{L}_2 = \frac{lh}{6} \begin{bmatrix} 2 & 1 \\ 1 & 2 \end{bmatrix}, \quad \underset{\sim}{M}_P = \frac{\rho l h^2}{216} \begin{bmatrix} 241 & 250 & 49 \\ 250 & 580 & 250 \\ 49 & 250 & 241 \end{bmatrix} \tag{33}$$

and $\underset{\sim}{M}_P$ may be transformed to give

$$\underset{\sim}{M}_P = \frac{\rho l h^2}{216} \begin{bmatrix} 540 & 0 & 0 \\ 0 & 1080 & 0 \\ 0 & 0 & 540 \end{bmatrix} \tag{34}$$

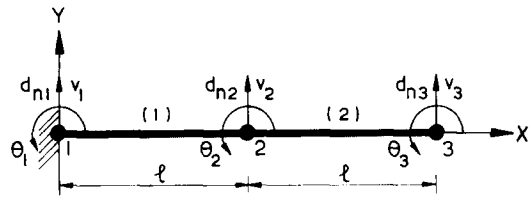

Fig. 5 Lateral vibration of underwater beam

which is called the *lumped mass matrix* of the fluid elements. This differs substantially from the approximate expression often used in preliminary engineering design, i.e., (Lu 1992)

$$\underset{\sim}{M}_P = \frac{\rho \bar{A} l}{2}\begin{bmatrix}1&0&0\\0&2&0\\0&0&1\end{bmatrix} = \rho l h^2 \begin{bmatrix}1&0&0\\0&2&0\\0&0&1\end{bmatrix} \tag{35}$$

Because the normal displacement $\underset{\sim}{d}_n$ at the interface with the fluid is coincident with the node deflections v of the beam, a co-ordinate transformation is not needed for this example, see Fig. 5.

The total set of degrees-of-freedom of the beam were ordered to give

$$\underset{\sim}{\bar{D}} = [v_1\ \theta_1\ v_2\ \theta_2\ v_3\ \theta_3]^T \tag{36}$$

The stiffness, compatibility and lumped mass matrices for the plane beam element are taken from Przemieniecki (1968). Hence, by assembling all of the elements and using the boundary conditions $v_1=\theta_1=0$, Eq. (29) becomes

$$\left\{\frac{EJ}{l^3}\begin{bmatrix}24&0&-12&6l\\0&8l^2&-6l&2l^2\\-12&-6l&12&-6l\\6l&2l^2&-6l&4l^2\end{bmatrix} - \omega^2\left(\frac{\rho_b l \bar{A}}{420}\begin{bmatrix}312&0&54&-13l\\0&8l^2&13l&3l^2\\54&13l&156&-22l\\-13l&-3l^2&-22l&4l^2\end{bmatrix} + \frac{\rho l h^2}{216}\begin{bmatrix}580&0&250&0\\0&0&0&0\\250&0&241&0\\0&0&0&0\end{bmatrix}\right)\right\}\begin{bmatrix}v_2\\\theta_2\\v_3\\\theta_3\end{bmatrix} = \underset{\sim}{0} \tag{37}$$

where the latter two matrices are the compatibility mass matrices for the beam and the fluid elements. Hence the first three natural frequencies are readily obtained as Ω_1=3.154, Ω_2=20.980 and Ω_3=80.737 where Ω_i is the normalised natural frequency defined as $\Omega_i=\omega_i L^2\sqrt{\rho_b \bar{A}/EJ}$, where ω_i is the i-th natural frequency of the beam.

Table 1 compares the values of Ω_1, Ω_2 and Ω_3 given above with those given by six other methods. Except for the results of column 1, the results were all obtained by the finite

Table 1 Normalised natural frequencies for first example, calculated by seven different methods

	Method						
	1	2	3	4	5	6	7
Ω_1	3.515	3.478	3.156	3.154	2.828	3.305	3.009
Ω_2	22.034	21.826	16.250	20.980	14.542	20.735	21.922
Ω_3	61.685	81.189	-	80.737	-	80.778	-

element solution presented in this paper but with the different assumptions listed below. Thus columns 1-7 correspond to:

(1) an analytical solution in which the influence of the fluid is ignored (Lin and Qu 1989);
(2) the influence of the fluid was ignored and the compatibility mass matrix was used for the beam elements;
(3) the influence of the fluid was again ignored but the lumped mass matrix was used for the beam elements;
(4) the compatibility mass matrices were used for both the beam and the fluid (i.e., Eq. (33)) elements (these are the assumptions which gave the values of Ω_1, Ω_2 and Ω_3 given beneath Eq. (37).);
(5) the lumped mass matrices were used for both the beam and the fluid (i.e., Eq. (34)) elements;
(6) the compatibility mass matrix was used for the beam elements and the approximate mass matrix of Eq. (35) was used for the fluid elements; and
(7) the lumped mass matrix was used for the beam elements and the approximate mass matrix was used for the fluid elements.

7.2. Example 2

Fig. 6(a) shows an accelerating underwater uniform simply-supported beam subjected to a central concentrated force $P \sin \theta t$, with P=10N and θ=0.01/s, and to a constant axial force F at its end. (The simple supports and F could result from the beam being attached to a parent structure which is accelerating with acceleration a parallel to the length of the beam). It has length L=2 m, mass per unit length m=25 kg/m, Young's modulus E=200 GN/m^2, moment of inertia $J=2\times10^{-5}$ m^4 and $F=Lma$, where a is the axial acceleration. The beam is uniformly divided into the 4 plane beam elements shown in Fig. 6(b).

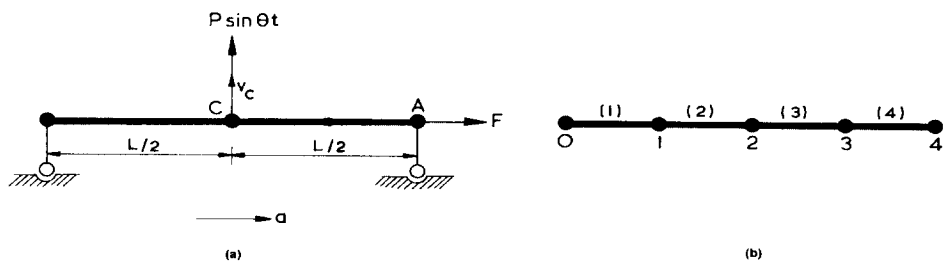

Fig. 6 Underwater motion of a simply-supported beam, showing the mesh used: (a) a simply-supported beam; (b) finite element mesh

Table 2 Normalised natural frequencies and deflection for second example

		Qian (1979)	a/g						
			0	0.1	1	100	−0.1	−1	−100
In air	Ω_1^*	9.8700	9.8721	9.8722	9.8723	10.7990	9.8721	9.8720	8.7740
	Ω_2^*	39.4800	39.6341	39.6341	39.6342	40.2411	39.6341	39.6340	39.0207
	V^*	2.105	2.080	2.055	2.050	1.725	2.055	2.060	2.580
In water	Ω_1^*	-	7.7211	7.7215	7.7216	8.4468	7.7115	7.7104	6.8625
	Ω_2^*	-	30.8932	30.8947	30.8948	31.3671	30.8947	30.8936	30.4171
	V^*	-	2.055	2.050	2.040	1.725	2.060	2.070	2.585

Table 2 compares the analytical solution of Qian (1979) for the beam in air with the results given by the method of this paper with the beam in either air or water and with a=0, 0.1 g, g, 100 g, −0.1 g, −g, or −100 g.

The acceleration of gravity, g, was approximated as g=10 m/s^2 and the additional water mass was represented by the approximate lumped mass method of Eq. (35). F was calculated from a by using Eq. (30), Ω^* is the normalised natural frequency and V^* is the normalised deflection amplitude at the centre of the beam, defined as

$$\Omega_i^* = \omega_i l^2 \sqrt{\frac{\rho m}{EJ}} \quad \text{and} \quad V^* = \frac{v_c}{L} \times 10^7$$

where ω_i is the i-th natural frequency and v_c is the deflection amplitude at the centre of the beam.

7.3. Example 3

Application of the theory to the free vibration and dynamic response of an accelerating underwater missile.

7.3.1. Model

The outer shape of the missile is shown in Fig. 7. Its body is a slender and thin cylindrical shell and the equation of the curve of the cowl at its head is known. The ratio of its length to diameter is 6 : 1. It is quite slender so that it can be modelled by a beam with varying circular cross-section. Since the material and cross-section vary in the axial direction, and its head is curved, the missile is divided into 17 elements in the axial direction. The cowl at its head

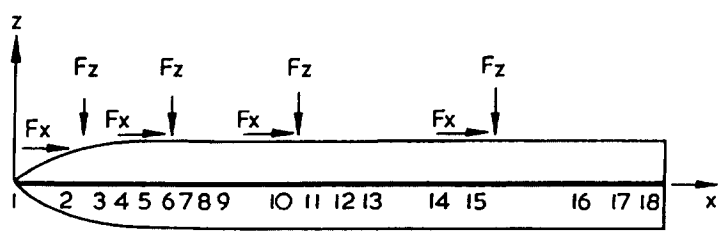

Fig. 7 Finite element model of a missile

Table 3 Dimensionless frequencies of free vibration

	ω_1^*	ω_2^*	ω_3^*	ω_4^*	ω_5^*	ω_6^*
in air	28.632	30.164	52.197	62.928	67.683	104.23
underwater	14.332	30.164	38.795	52.197	55.598	70.848

involves 6 elements. This cowl contributes to the stiffness and mass matrices, and the head part of the missile can be considered as a double-layered shell.

The material and geometrical properties of the elements vary within the following bounds:

ν=0.3~0.33, E=11.9~210 GN/m^2

Thickness δ=0.001~0.017 m

Second moment of area $J_y=J_z=J_x/2=1.755\times10^{-3}$~$5.204\times10^{-2}$ m^4

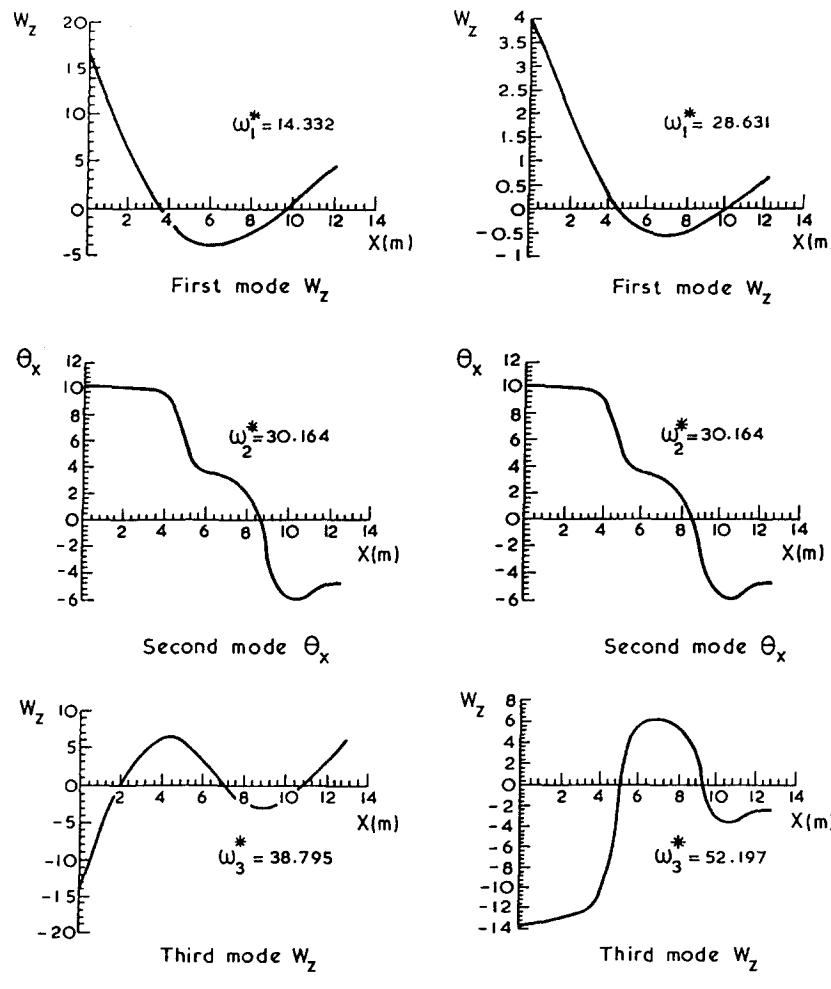

Fig. 8 Principal modes corresponding to ω_1^*, ω_2^* and ω_3^* for the missile: (a) underwater; (b) in air

Table 4 Maximum internal forces in the missile

	Axial force N_x^*			Shear force Q_z^*			Bending moment M_y^*		
	Value	Position (m)	Time (s)	Value	Position (m)	Time (s)	Value	Position (m)	Time (s)
In air	716.958	3.461	0.61	21.166	8.548	0.61	35.845	4.069	0.61
Underwater	692.020	3.461	0.61	12.531	8.548	0.61	17.176	3.461	0.61

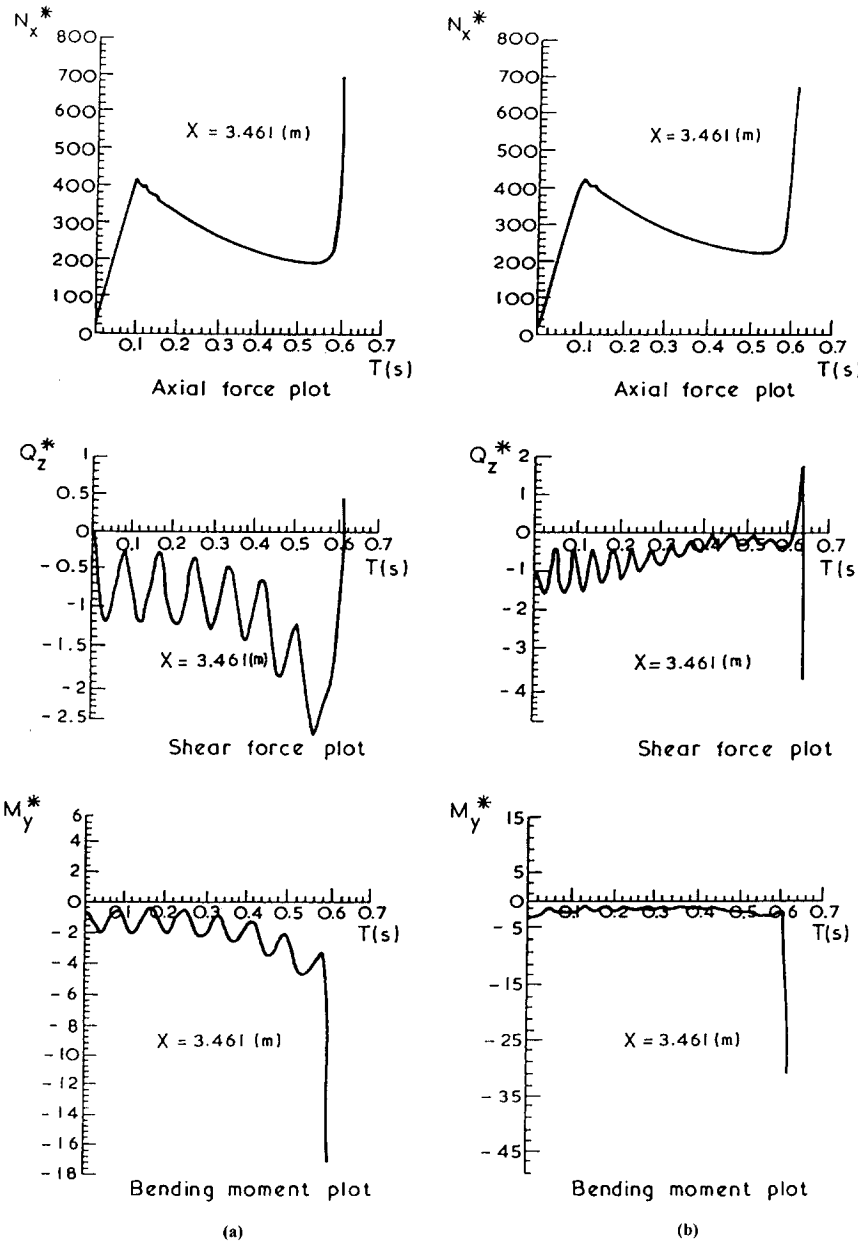

Fig. 9 Temporal variations of the internal forces at x=3.461m for the missile: (a) underwater; (b) in air

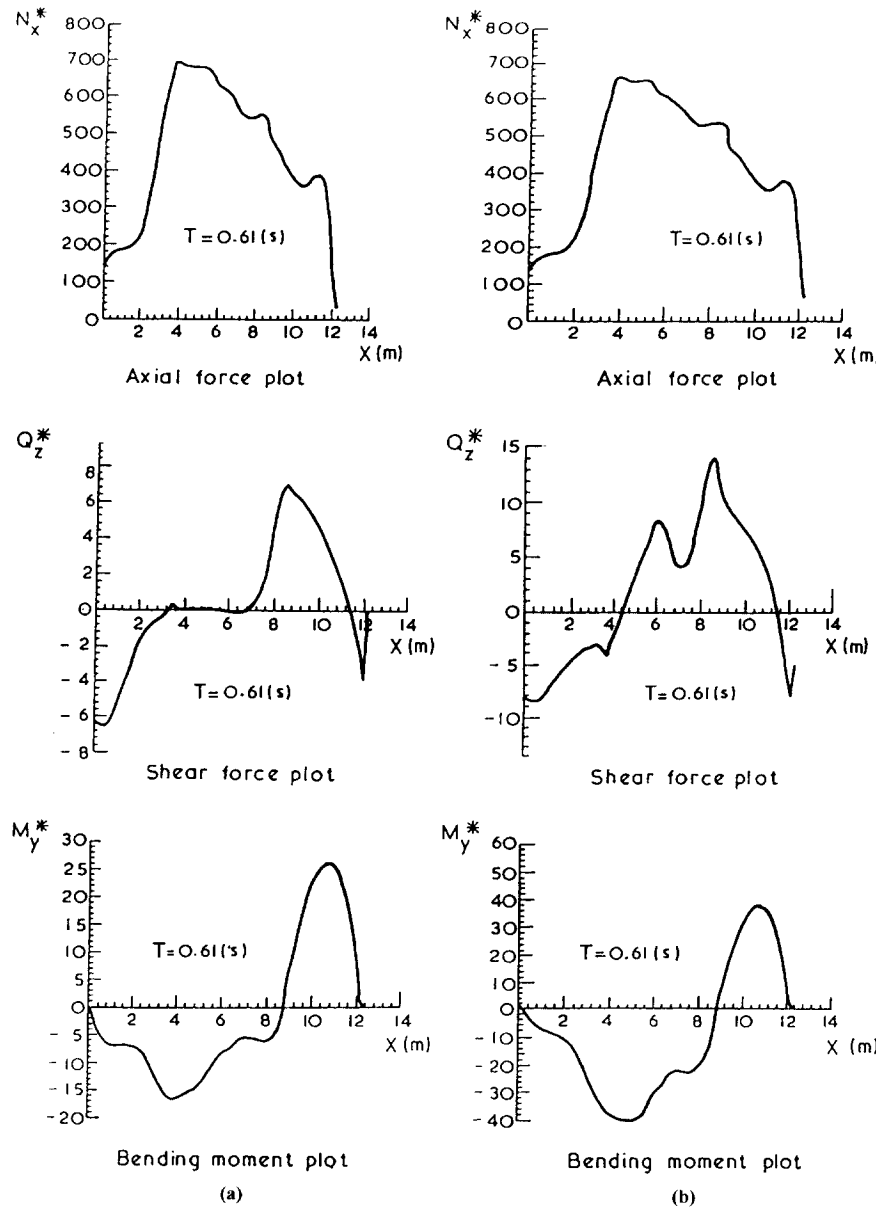

Fig. 10 Axial distributions of the internal forces at T=0.61s for the missile: (a) underwater; (b) in air

7.3.2. Frequencies and modes of the vibration of the missile moving in air or underwater

Let the dimensionless circular frequency

$$\omega^* = \frac{\omega}{\frac{1}{L^2}\sqrt{\frac{EJ}{\rho_b \bar{A}}}}$$

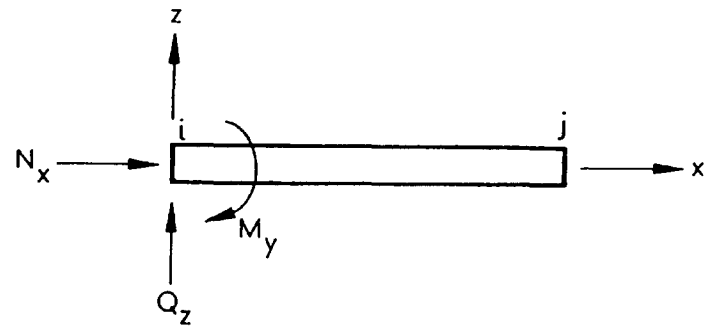

Fig. 11 Sign convention for the internal forces

be introduced, where L is the length, E is the mean Young's modulus, J is the mean second moment of area, ρ_b is the mean mass density and $\bar{A}$ is the mean cross-sectional area of the missile.

The first six values of ω^* of the missile accelerating in air or underwater are listed in Table 3, from which it can be seen that ω_1^* underwater is only one half of ω_1^* in air because of the water/structure coupling. In contrast, ω_2^* is the same in both cases since it is a frequency of rotational vibration, with the mass of adhering water neglected.

The first three principal modes corresponding to ω_1^*, ω_2^* and ω_3^* for both the in air and underwater cases are shown in Fig. 8.

7.3.3. Dynamic response of a missile moving in air or underwater

Define the following dimensionless quantities:

$$N_x^* = \frac{N_x}{\left(\frac{\bar{A}EJ}{L^4}\right)}, \quad Q_z^* = \frac{Q_z}{\left(\frac{\bar{A}EJ}{L^4}\right)}, \quad M_y^* = \frac{M_y}{\left(\frac{\bar{A}EJ}{L^3}\right)}$$

where N_x is the axial force, Q_z is the shear force in the z-direction and M_y is the bending moment about the y-axis.

The maximum absolute values of N_x^*, Q_z^* and M_y^*, their positions (as values of x) and the time of their occurrence are listed in Table 4. It can be seen that the coupling between the water and the structure causes the maximum values of the internal forces (especially the shear force and bending moment) to be reduced, but that it leaves the time of the occurrence of the maximum values unaffected.

Fig. 9 shows the temporal variations of N_x^*, Q_z^* and M_y^* at x=3.461 m and Fig. 10 gives the axial distributions of N_x^*, Q_z^* and M_y^* at T=0.61 s. The positive directions of N_x^*, Q_z^* and M_y^* are defined as in Fig. 11, i.e., if a force vector or a moment vector coincides with the positive direction of the corresponding coordinate axis, it is defined as positive, otherwise negative.

8. Conclusions

The first example was chosen to be very small and also artificial, so that it could be solved

by hand to give more insight into the methods considered in this paper. The second example is also small, but used a small computer program. However, several largely predictable conclusions may be drawn from Tables 1 and 2, as follows: (1) the precision given by the compatibility mass matrix is higher than that given by the lumped mass matrix; (2) because so few elements were used only the lower order natural frequencies approach the analytical solution; (3) the natural frequencies decrease when the influence of additional water mass is considered, with the lower order natural frequencies being more affected than the higher ones; and (4) the natural frequencies are increased by the inertial acceleration when it is positive, or are reduced when it is negative.

Example 3 shows the capability of the method in dealing with the free vibration and dynamic response of an accelerating underwater missile. Table 3 shows that the first frequency parameter of the missile underwater is half of that in air, due to the water/structure coupling, whereas the second frequency parameter is the same for the missile underwater and in air as it corresponds to a rotational vibration, with the mass of adhering water neglected. Table 4 shows that the water/structure coupling causes a reduction in the values of the internal forces, while the time of the occurrence of the maximum values remains unaffected.

Acknowledgements

This study was supported in part by the Foundation for Promoting cultural, educational and technical co-operation between Britain and China and also by the Cardiff Advanced Chinese Engineering Centre.

References

Betts, C.V., Bishop, R.E.D. and Price, W.G. (1977), "The symmetric generalised fluid forces applied to a ship in a seaway", *Trans. RINA,* **119**, 265-278, U.K.

Bishop, R.E.D., Clarke, J.D. and Price, W.G. (1984), "Comparison of full scale and predicted responses of two frigates in a severe weather trial", *Trans. RINA,* **126**, 153-166, U.K.

Bishop, R.E.D., Eatock Taylor, R. and Jackson, K.L. (1973), "On the structural dynamics of ship hulls in waves", *Trans. RINA,* **115**, 257-274, U.K.

Bishop, R.E.D. and Price, W.G. (1974), "On modal analysis of ship strength", *Proceedings of the Royal Society, London,* **A341**, 121-134.

Bishop, R.E.D. and Price, W.G. (1979), *Hydroelasticity of Ships*, Cambridge University Press, London.

Block, J.J. and Beukelman, W. (1984), "The high-speed displacement ship systematic series hull forms – seakeeping characteristics", *SNAME Trans.,* **92**, 125-150.

Chang, M.S. (1977), "Computations of three-dimensional ship motions with forward speed", *Proceedings of 2-nd Int. Conf. Num. Ship Hydrodynamics*, 124-135, Univ. of California, Berkeley.

Chang, M.S. and Pien, P.C. (1976), "Velocity potentials of submerged bodies near free surface – application to wave-excited forces and motions", *Proceeding of 11-th Symposium on Naval Hydrodynamics.*

Clarke, J.D. (1986), *Wave Loading in Warships, Advances in Marine Structures*, Ed. by C.S. Smith and J.D. Clarke, Elsevier Applied Science Publishers, 1-25.

Ertekin, R.C., Riggs, H.R., Che, X.L. and Du, S.X. (1993). "Efficient methods for hydroelastic analysis of very large floating structures", *J. of Ship Research,* **37**(1), 58-76.

Faltinsen, O. and Michelsen, F.C. (1974), "Motions of large structure in waves at zero froude number", *Proceedings of 1-st Symp. Dyn. Mar. Vehicles & Struct. Waves*, 91-106.

Guevel, P. and Bougis, J. (1982), "Ship-motions with forward speed in infinite depth", *Int. Shipbuilding progress,* **29**(332), 103-117.
Haskind, M.D. (1946a), "The hydrodynamic theory of ship oscillations in rolling and pitching", *Prikl. Mat. Mekh,* **10**, 33-36. (Engl. Transl., Tech. Res. Bull., No. 1-12, 3-43, SNAME, New York, 1953).
Haskind, M.D. (1946b), "The oscillations of a ship in still water", *Izv. Akad. Nauk. SSSR. Otd. Tekh. Nauk,* **1**, 23-34. (Engl. Transl., Tech. Res. Bull., No. 1-12, 45-60, SNAME, New York, 1953).
Holand, I. and Bell, K. (1972), *Finite Element Method in Stress Analysis*, TAPIR, The Technical University of Norway.
Inglis, R.B. and Price, W.G. (1982), "A three dimensional ship motion theory – comparison between theoretical predictions and experimental data of the hydrodynamic coefficients with forward speed", *Trans. RINA,* **124**, 141-157, U.K.
Kabaila, A.P. (1970), *Bifurcation of Space Frames*, AFFDL-TR-70-36.
Kagemoto, H. and Yue, D.K.P. (1993), "Hydrodynamics interaction analysis of very large floating structures", *Marine Structures,* **6**(2 and 3), 295-322.
Korsmeyer, F.T., Lee, C.H., Newman, J.N. and Sclavounos, P.D. (1988), "The analysis of wave effects on tension-leg platforms", *OMAE, Houston, Texas,* **2**, 1-14.
Korvin-Kroukovsky, B.V. and Jacobs, W.R. (1957), "Pitching and heaving motions of a ship in regular waves", *SNAME Trans.,* **65**, *590-632.*
Lamb, H. (1920), "On the vibration of an elastic plate in contact with water", *Proceedings of the Royal Society, London,* **98**(A 690), 205-215.
Lin, Jiahao and Qu, Naisi (1989), *Computational Structural Dynamics*, Higher Education Press (in Chinese).
Lu, Xingshen (1992), *Advanced Structural Dynamics*, Shanghai Jiao Tong University Press (in Chinese).
Lundgren, J., Price, W.G. and Wu, Y.S. (1988), "A hydroelastic investigation into the behaviour of a floating 'Dry' dock in waves", *Proceedings of Spring Meetings, RINA, London.*
Mays, J.H. (1978), *Wave Radiation and Diffraction by a Floating Slender Body*, Ph.D. Thesis, MIT., Cambridge, Massachusetts.
Newman, J.N. (1964), "A slender-body theory for ship oscillations in Waves", *J. of Fluid Mechanics,* **18**, 602-618.
Newman, J.N. (1978a), *Marine Hydrodynamics*, The MIT Press, Cambridge, Massachusetts.
Newman, J.N. (1978b), "The theory of ship motions", *Advances in Applied Mechanics,* **18**, 221-283.
Newman, J.N. and Sclavounos, P.D. (1980), "The unified theory of ship motions", *Proceedings of 13-th ONR*, Tokyo.
Ogilvie, T.F. and Tuck, E.O. (1969), "A rational strip theory for ship motions", *Part 1, Report No. 013*, University of Michigan.
Przemieniecki, J.S. (1968), *Theory of Matrix Structural Analysis*, McGraw-Hill Book Company, London.
Qian, Biafeng (1979), *The Structure Dynamics*, China Building Engineering Press (in Chinese).
Salvesen, N., Tuck, E.O. and Faltinsen, O. (1970), "Ship motions and sea loads", *SNAME Trans.,* **78**, 250-287.
Sclavounos, P.D. (1981), *On the Diffraction of Free-Surface Waves by a Slender Ship*, Ph.D. Thesis, MIT, Cambridge, Massachusetts.
Sclavounos, P.D. (1984), "The diffraction of free-surface waves by a slender ship", *J. of Ship Research,* **28**(1), 29-47.
Sclavounos, P.D. (1985), "The unified slender-body theory: ship motions in waves", *Proceedings of 15-th ONR*, Hamburg.
Ursell, F. (1949), "On the heaving motion of a circular cylinder on the surface of a fluid", *Quarterly Journal of Mech. and Applied Math.,* **2**(2), 218-231.
Ursell, F. (1962), "Slender oscillating ships at zero forward speed", *J. of Fluid Mechanics,* **14**(4), 496-516.
Wu, Y.S. (1984), *Hydroelasticity of Floating Bodies*, Ph.D. Thesis, Brunel University, U.K.
Zienkiewicz, O.C. (1977), *The Finite Element Method*, McGraw-Hill Book Company, London.